MATERIALS AND SYSTEMS
FOR QUANTUM OPTICS

10-mJ Optically Synchronized CEP-Stable Chirped Parametric Amplifier at 1.5 μm[1]

O. D. Mücke[a], D. Sidorov[a], P. Dombi[a], A. Pugžlys[a], S. Ališauskas[b], V. Smilgevičius[b], N. Forget[c], J. Posius[d], L. Giniūnas[d], R. Danielius[d], and A. Baltuška[a]

[a] *Photonics Institute, Vienna University of Technology, Vienna, A-1040 Austria*
[b] *Laser Research Center, Vilnius University, Vilnius, LT-10223 Lithuania*
[c] *Fastlite, Bâtiment 403, Ecole Polytechnique, Palaiseau, 91128 France*
[d] *Light Conversion Ltd., P/O Box 14-85, Vilnius, LT-10223 Lithuania*
e-mail: oliver.muecke@tuwien.ac.at, baltuska@tuwien.ac.at
Received August 3, 2009

Abstract—We demonstrate the generation of 10-mJ 1.5-μm few-cycle pulses from a 4-stage OPCPA system. The system is based on a fusion of femtosecond DPSS Yb technology and a picosecond Nd:YAG pump laser. In a first preliminary filamentation experiment in argon at 5 atm, we observe significant spectral broadening of the recompressed multi-mJ 1.5-μm pulses. The filamentation output spectrum supports the generation of 8 fs pulses equivalent to sub-to-cycle pulses at 1.5 μm. We foresee that our terawatt-peak-power sub-to-cycle pulse source will open the door to exciting new experiments in attosecond high-field science in the near future.

INTRODUCTION

Optical Parametric Chirped-Pulse Amplification (OPCPA) [1] has attracted a lot of attention as a promising route toward intensity scaling of few-cycle laser pulses. Intense phase-stable few-cycle laser pulses have numerous intriguing applications in attosecond science and high-field science including attosecond XUV/soft-X-ray pulse generation by high-harmonic generation (HHG) [2–4], tomographic imaging of molecular orbitals [5], and laser-induced electron diffraction [6]. A major challenge for using HHG in studies of time-resolved tomography of molecular dissociative states is the low ionization potential I_p of excited molecular states. The resulting competition between state depletion and HHG prevents generation of broad HHG spectra necessary for tomographic reconstruction. One solution are laser sources with high ponderomotive energy $U_p \propto \lambda^2 I$ at moderate intensity level, i.e., infrared phase-stable few-cycle high-power laser systems. High-U_p-sources [7–9] also open the door to experimental investigations of the λ-scaling laws of strong-field physics [10, 11] (Keldysh parameter $\propto \lambda^{-1}$, electron energies $\propto \lambda^2$, HHG cutoff $\propto \lambda^2$, HHG efficiency $\propto \lambda^{-5.5}$, minimum attosecond pulse duration $\propto \lambda^{-1/2}$), and they would benefit laser-induced electron diffraction because of the shorter de Broglie electron wavelength and consequently higher spatial resolution [6]. Recent work on phase matching

of higher harmonics driven by IR pulses [12–16] have pointed out that for longer-wavelength driver pulses favorable phase matching conditions might be achievable that could mitigate the unfavorable $\lambda^{-5.5}$-scaling of the HHG efficiency in single-atom response. Thus, phase-matched HHG driven by intense few-cycle IR pulses represents a promising route towards bright coherent sources in the soft and hard X-ray regions.

The main objective of our work is to generate IR pulses with ~40 fs duration that fully satisfy the requirements for external spectral broadening in gas [17, 18]. In addition, with an IR pulse we expect to surpass the energy limitation (4–5 mJ at 0.8 μm) for gas broadening schemes because the critical power of self-focusing also scales as λ^2.

Using mJ pulses from Ti:sapphire amplifiers at 0.8 μm, coherent X-rays in the keV photon energy range were generated by HHG in helium [19]. A technological problem hindering further progress is gas ionization in the gas-filled hollow-fiber compressors required to achieve few-cycle pulse duration at pulse energies >1 mJ. More fundamentally, helium already saturates for intensities >1 PW/cm² and few-cycle pulses at 0.8 μm, thus the HHG cutoff and photon flux is limited by ground-state depletion in helium in these experiments.

Here, we report on the development of a multi-mJ all-optically synchronized and phase-stable OPCPA at 1.5 μm [20, 21]. As opposed to our OPCPA system developed earlier [7], in this work we pursue a novel

---

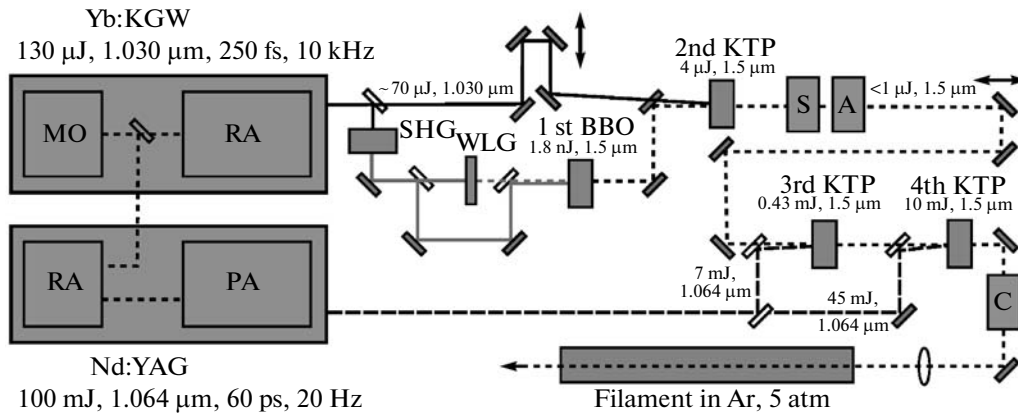[1] The article is published in the original.

Fig. 1. Scheme of the IR OPCPA setup: master oscillator (MO), regenerative amplifier (RA), double-pass post amplifier (PA), Grating-based stretcher/compressor (S/C), acousto-optic programmable dispersive filter DAZZLER (A), white light generator (WLG) in a 10-mm-thick sapphire plate. The passively CEP-stable idler wave from stage 1 becomes the signal wave in stage 2. Stage 1 (Type I BBO) is pumped at 515 nm, stage 2 (Type II KTP) at 1.030 μm, stages 3 and 4 (Type II KTP) at 1.064 μm.
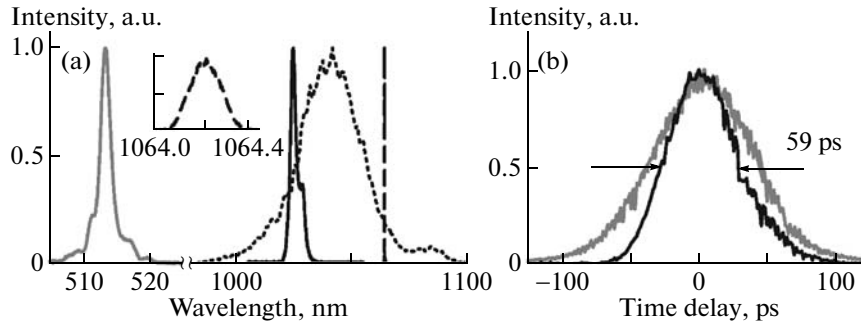
Fig. 2. Synchronization of the Yb:KGW and Nd:YAG amplifiers. (a) Laser spectra: Kerr lens mode-locked Yb:KGW oscillator (dotted curve), Yb:KGW regenerative amplifier (black solid), Nd:YAG with an intracavity 2-mm-thick etalon (dashed), and SHG of Yb:KGW (grey). (b) Pulse measurement of the picosecond Nd:YAG amplifier, showing an autocorrelation (AC, gray line) and a cross-correlation (XC, black line) between the Yb:KGW (~200-fs) and Nd:YAG.

technological route: (1) with the advent of a mature 200-fs Yb MOPA system it became possible to abandon the Ti:sapphire front-end; (2) we avoid working close to the signal-idler wavelength degeneracy and reduce the quantum defect for the signal wave; (3) we employ (nearly) collinear Type-II phase matching that, as opposed to Type I supports a much narrower bandwidth but is free of parasitic self-diffraction [22]. Following the pioneering work of Miller and coworkers [23, 24], we employ Type-II KTP/KTA (1.030/1.064 μm pump, ~1.5 μm signal, ~3.3−3.7 μm idler) because these crystals are transparent for the mid-IR idler wavelength and exhibit a relatively broad bandwidth around 1.5 μm.

2. MULTIMILLIJOULE INFRARED FEW-CYCLE OPCPA

In our experimental scheme shown in Fig. 1, both Yb and Nd regenerative amplifiers (RAs) are simulta-neously seeded from a single master oscillator that has a modest FWHM bandwidth of 30 nm (see Fig. 2). To seed the Nd RA, we pick up the zeroth-order diffraction beam behind a transmission grating in the pulse stretcher. The repetition rate of the Yb:KGW DPSS MOPA (Pharos, Light Conversion, Ltd.), tunable in the range of 1−100 kHz, was set at 10 kHz as the 500th harmonic of the flash-lamp-pumped Nd:YAG, amplifier (Ekspla Ltd.) operating at 20 Hz. In the Nd RA, an intracavity etalon is used to narrow the pulse bandwidth and make the pulse duration safe for post amplification (see Fig. 2).

The 1.03 μm output from the femtosecond Yb:KGW MOPA is first split into two parts by means of a variable beam splitter (consisting of a half-wave-plate and a thin-film polarizer); part one is used for implementing the 1st OPA stage, part two is used for pumping the 2nd OPA stage. In the 1st OPA stage, the 1.03 μm pulses are first frequency doubled in a 1-mm-thick Type-I BBO crystal ($\theta = 23.4°$, $\phi = 90°$). Typi-
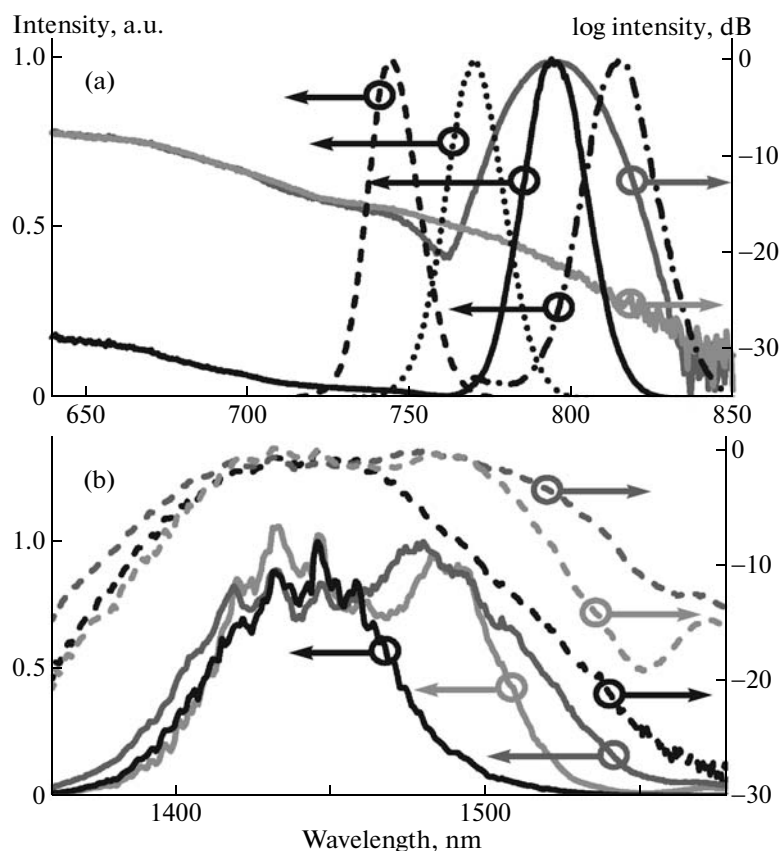
Fig. 3. Spectral properties of the 1st and 2nd OPA stages. (a) NIR WLG seed (light grey curve) and signal spectra (grey and black solid) of the 1st OPA stage. The dashed and dotted curves indicate tunability of the 1st stage signal (and idler). (b) Infrared CEP-stable seed (black), amplified 2nd stage signal (grey), spectrum measured before the FROG setup (light grey).

cally 8.5 μJ of 515 nm pulses are again split by a variable beam splitter into two parts: 1.3 μJ (measured behind a variable aperture used for fine-adjusting the input beam diameter) are focused onto a 10-mm-thick sapphire plate using an 87-mm focusing lens. In the sapphire plate, a stable white light continuum extending to wavelengths >840 nm (see Fig. 3a) is created in a single filament. The white light continuum, which is recollimated with a 40-mm lens, is used to seed the 1st OPA stage. The white light seed pulses and the 515 nm pump pulses are combined *collinearly* (to avoid idler angular dispersion) on a dichroic beam splitter and both focused onto a 4-mm-thick Type-I BBO crystal ($\theta = 22.8°$, $\phi = 90°$) with an $f = 20$ cm spherical mirror to a $1/e^2$ pump beam diameter of 120 μm. In the pump beam, a variable aperture is used to adjust the pump energy to 1.4 μJ (thus, the parametric gain) and to minimize the detrimental effects of amplified spontaneous emission. By adjusting both the θ-angle of the BBO crystal and time delay between the seed and pump pulses, different wavelength regions can be phase matched for efficient parametric amplification (see Fig. 3a). In particular, selecting the ~795 nm wavelength for amplification, this configuration pro-

duces CEP-stable idler pulses [25] at 1.44 μm (Fig. 3b) that we use as seed in the 2nd OPA stage.

For the amplification stages 2–4, we employ Type-II KTP/KTA crystals (1.030/1.064 μm pump, ~1.5 μm signal, ~3.3–3.7 μm idler) because these crystals (unlike BBO, BIBO, and LBO) are transparent for the mid-IR idler wavelength and exhibit a relatively broad bandwidth around 1.5 μm. The CEP-stable idler pulses from the 1st OPA stage (i.e., the seed pulses for the 2nd OPA stage) are recollimated with a 10-cm lens and focused onto a 6-mm-thick Type-II KTP crystal ($\theta = 45.5°$, $\phi = 0°$), using a 50-cm lens. The pump beam is focused onto the same KTP crystal using a 100-cm lens under an (external) walk-off compensation angle of 2.1° with respect to the seed beam. For a pump beam diameter of ~550 μm measured at the KTP crystal input face and 69 μJ (measured behind a variable aperture) pump pulses, we achieve 4 μJ signal pulses, i.e., a pump-signal conversion efficiency of ~6% in the 2nd OPA stage. The pulse-to-pulse intensity fluctuations of the two-stage OPA amounts to 2.5% rms noise, only two times larger than that of the Yb:KGW MOPA pump (1.2% rms). The far-field beam profile of the 2nd-stage signal wave shown in Fig. 6b is nearly Gaussian; the beam propa-

gation factor was determined to be $M^2 = 1.13 \pm 0.04$ as compared to $M^2 < 1.2$ of the pump.

The strong nonlinear optical Kerr effect in KTP/KTA (nonlinear refractive index coefficient $n_2(\text{KTP/KTA}) = 23.7 \times 10^{-16}$ cm²/W as compared to $n_2(\text{BBO}) = 2.9 \times 10^{-16}$ cm²/W [26]) raises the important question how severe is pump/idler-to-signal cross-phase modulation (XPM) in the 2nd OPA stage and its effect on CEP stability. The nonlinear effects accumulated during the OPA process in a nonlinear crystal of length L can be quantified by introducing a generalized B-integral

$$ B = \frac{2\pi n_2}{\lambda_s} \int_0^{} dz [I_s(z) + \gamma_{sp} I_p(z) + \gamma_{si} I_i(z)]. \quad (1) $$

The coefficients γ_{sp} and γ_{si}, which quantify the pump-signal and idler-signal coupling, are 2 for parallel polarizations and 2/3 for orthogonal polarizations [27]. The resulting values of the coupling coefficients for three types of phase matching in the XZ-plane ($\phi = 0°$) in KTP/KTA OPAs are summarized in the table. Obviously, Type II ($e_s + o_i \longrightarrow o_p$) phase matching as used in our amplification stages 2–4 minimizes the detrimental XPM contribution of pump and idler on the signal wave.

CEP stability of the 2nd OPA output was investigated by means of inline f-to-$2f$ interferometry in the wavelength range from 650–790 nm (see Fig. 4). The observation of stable interference fringes directly proves CEP stability and negligible influence of XPM on the CEP. Note that OPCPA in the 3rd and 4th OPA stages preserve CEP stability of the seed pulses. The slow CEP drift observed in Fig. 4 is clearly of environmental origin and can easily be compensated for by

Phase-matching types in the XZ-plane in KTP/KTA OPAs and corresponding XPM coupling coefficients γ_{sp} and γ_{si}

Phase-matching type	γ_{sp}	γ_{si}
Type I ($e_s + e_i \longrightarrow o_p$)	2/3	2
Type II ($e_s + o_i \longrightarrow o_p$)	2/3	2/3
Type III ($o_s + e_i \longrightarrow o_p$)	2	2/3

feedback stabilization of the interferometer formed by the seed- and pump-paths in the 1st OPA stage (see Fig. 1).

This CEP-stable μJ-level two-stage OPA based on a DPSS femtosecond Yb:MOPA system represents an attractive alternative to traditional Ti:sapphire-based front-ends (e.g., [7−9]) for seeding multi-mJ OPCPA systems. In order to demonstrate this, the 2nd-stage signal pulses are stretched to ~40 ps and again recompressed to sub-40 fs duration using a grating-based stretcher/compressor pair (500 grooves/mm plane ruled 96%-efficient gold reflection gratings, blazed for 1.37 μm with nominal blaze angle of 20°) [28] and an infrared high-resolution acousto-optic programmable dispersive filter (AOPDF, DAZZLER by Fastlite) [29]. Figure 5 shows SHG-FROG measurements of 1.47 μm pulses with 92 nm FWHM bandwidth from the 2nd OPA stage after stretching to ~40 ps and recompression to a FWHM 33 fs pulse duration.

The temporally stretched 2nd-stage signal (i.e., the 3rd-stage seed) is amplified in two final OPCPA stages (3rd and 4th employing 10-mm-thick Type-II KTP crystals) using a 90-mJ picosecond pump pulse from the Nd:YAG system (Fig. 6a). The maximum energy of the signal pulses at 1.55 μm before recompression is ~10 mJ. As the output from the 4th OPA stage exhibits
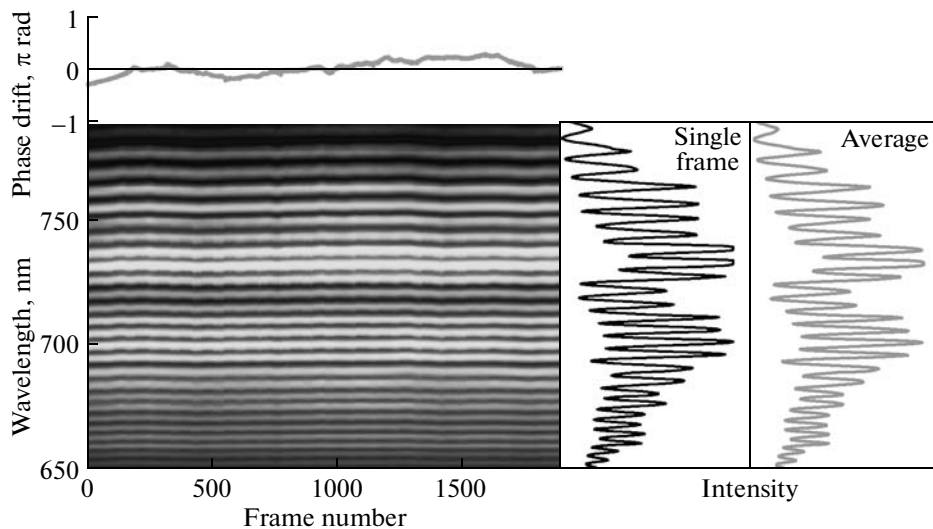

Fig. 4. f-to-$2f$ interferogram exhibiting stable fringes due to CEP stability. The black and grey curves on the right panels indicate the spectra averaged over 1900 frames (2 ms frame exposure time) and a single frame, respectively, on the same intensity axis. The grey curve in the above panel indicates the extracted phase drift of the 2nd stage signal.
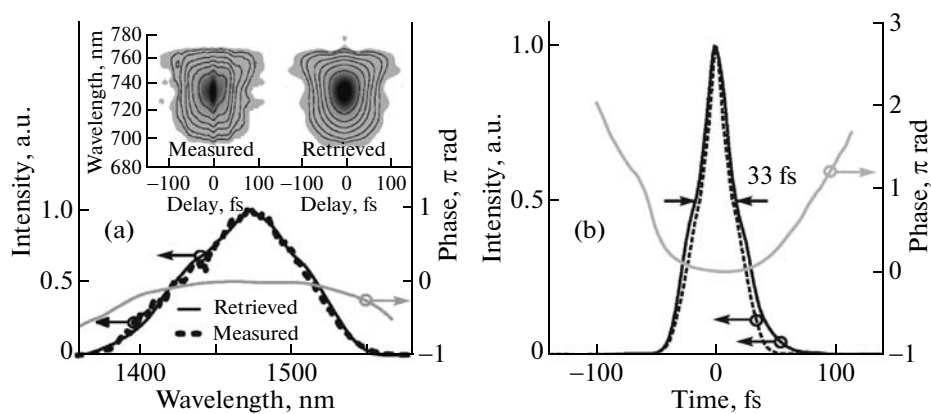
Fig. 5. SHG-FROG characterization of stretched and recompressed 1.47 μm pulses from the 2nd OPA stage. (a) Measured spectrum (black dashed curve), retrieved spectral intensity (black) and phase (grey). The insets show the measured and retrieved FROG traces. (b) Retrieved temporal intensity (black) and phase (grey) profiles indicating a 33-fs FWHM pulse duration. The transform-limited intensity profile (black dashed) corresponds to a 28 fs duration.
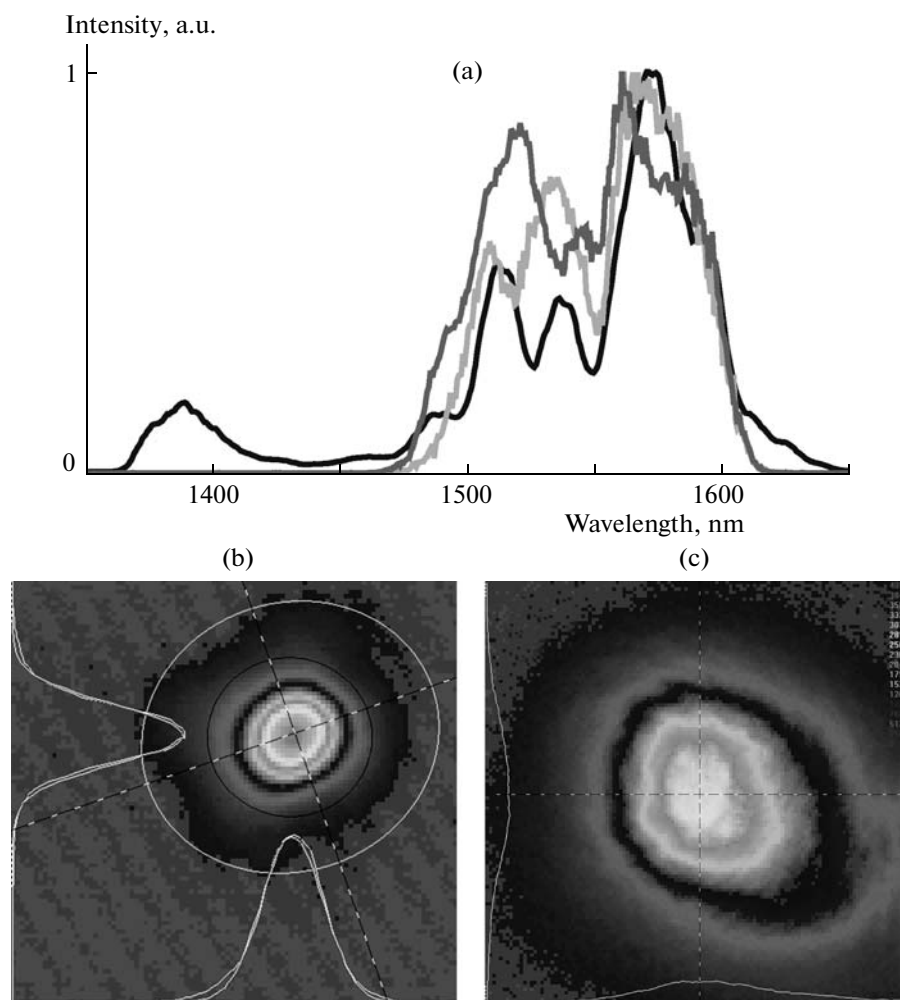

Fig. 6. (a) Spectral properties of the power amplification stages: spectrum of the 3rd-stage seed (black curve), and amplified signal spectra after the 3rd (light grey) and 4th (grey) amplification stages. (b) Far-field beam profile of the 2nd-stage signal wave (grey-scale false-color plot). (c) Beam profile of the multi-mJ signal wave after 5× magnification with a Galilean beam expander before recompression.
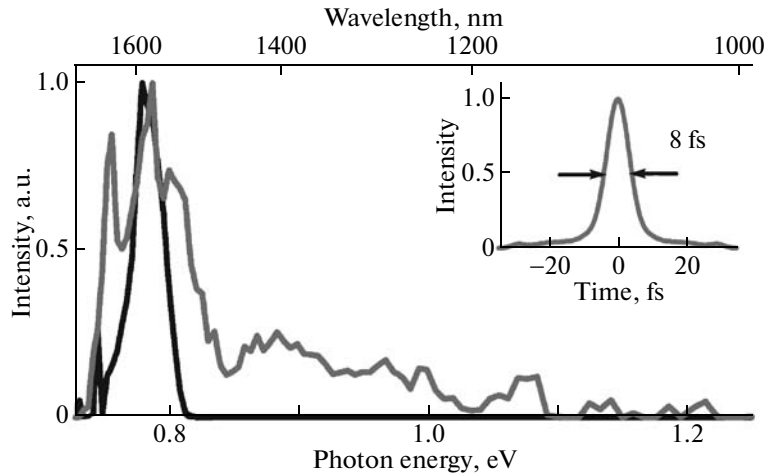
Fig. 7. Filamentation of recompressed 2.5-mJ 1.6-μm pulses in argon at 5 atm: Individually normalized input (black curve) and output spectra (grey) of the filamentation experiment. The inset shows the transform-limited intensity profile computed from the output spectrum.

a spectral bandwidth comparable to the 2nd OPA stage (Fig. 5a), we are confident that the multi-mJ-level output from the power amplification stages is recompressible to comparable pulse durations.

The $1/e^2$-beam diameter of the 4th stage output is widened by a factor of 5 to 9.5 mm by means of a Galilean beam expander in order to avoid damaging of the gold grating in the compressor.

FILAMENTATION IN ARGON

After recompressing the 4th-stage signal pulses we performed a preliminary filamentation experiment (Fig. 7). In this first experiment, we only used 2.5-mJ pulses at 1.6 μm in order to ensure a single filament under the current experimental conditions. These pulses are focused into a 138-cm long gas cell filled with argon (15.76 eV ionization potential) at 5 atm pressure using a 50-cm lens placed 4-cm in front of the gas cell. The input window of the cell has an antireflection coating covering the input pulse spectrum, the output window is a standard BK7 window. The preliminary results shown in Fig. 7 exhibit significant spectral broadening of the 1.6-μm pulses. The inset in Fig. 7 shows the transform-limited intensity profile computed from the output spectrum which indicates an 8 fs pulse duration, i.e., less than two optical cycles at 1.5 μm.

CONCLUSIONS AND OUTLOOK

In conclusion, we have demonstrated 10-mJ CEP-stable parametric amplification at ~1.5 μm based on a fusion of a DPSS femtosecond Yb-MOPA system and picosecond Nd:YAG solid-state technology. In a first preliminary filamentation experiment in argon at 5 atm, we have observed significant spectral broadening of the recompressed output from the 4-stage parametric amplifier. The resulting output spectrum supports the generation of 8 fs pulses, i.e., sub-two-cycle pulses at 1.5 μm. Current work aims to further optimize the recompression of the 20-Hz multi-mJ output pulses using the DAZZLER and to optimize the filamentation with respect to spectral broadening and energy throughput by varying the parameters pulse energy and chirp, beam diameter, focusing, gas type and pressure. Ultimately, with our 1.5 μm-pulses we expect to surpass the energy limitation (4–5 mJ at 0.8 μm) for gas broadening schemes because the critical power of self-focusing scales as λ^2 [18]. Characterization of the filamentation output pulses is already under way. We foresee that our terawatt-peak-power sub-two-cycle pulse source will open the door to exciting new experiments in attosecond high-field science in the near future.

Note Added in Proof

Since submission of this paper, we successfully recompressed 3.5-mJ, 1.57-μm pulses with 62 nm bandwidth from the 20-Hz four-stage IR OPCPA to a 74.4-fs pulse duration [21]. Moreover, we achieved self-compression of CEP-stable 2.2-mJ, 74.4-fs, 1.57-μm pulses down to 19.8 fs duration in a single filament in argon with 1.5 mJ output energy and a 66% energy throughput [21].

ACKNOWLEDGMENTS

REFERENCES

1. A. Dubietis, R. Butkus, and A. P. Piskarskas, IEEE J. Selected Topics Quantum Electron. **12**, 163 (2006) (and references therein).

2. M. Hentschel, R. Kienberger, C. Spielmann, G. A. Reider, N. Milosevic, T. Brabec, P. Corkum, U. Heinzmann, M. Drescher, and F. Krausz, Nature **414**, 509 (2001).

3. R. Kienberger, E. Goulielmakis, M. Uiberacker, A. Baltuška, V. Yakovlev, F. Bammer, A. Scrinzi, T. Westerwalbesloh, U. Kleineberg, U. Heinzmann, M. Drescher, and F. Krausz, Nature **427**, 817 (2004).

4. G. Sansone, E. Benedetti, F. Calegari, C. Vozzi, L. Avaldi, R. Flammini, L. Poletto, P. Villoresi, C. Altucci, R. Velotta, S. Stagira, S. De Silvestri, and M. Nisoli, Science **314**, 443 (2006).

5. J. Itatani, J. Levesque, D. Zeidler, H. Niikura, H. Pépin, J. C. Kieffer, P. B. Corkum, and D. M. Villeneuve, Nature **432**, 867 (2004).

6. M. Meckel, D. Comtois, D. Zeidler, A. Staudte, D. Pavičić, H. C. Bandulet, H. Pépin, J. C. Kieffer, R. Dörner, D. M. Villeneuve, and P. B. Corkum, Science **320**, 1478 (2008) (and references therein).

7. T. Fuji, N. Ishii, C. Y. Teisset, X. Gu, Th. Metzger, A. Baltuška, N. Forget, D. Kaplan, A. Galvanauskas, and F. Krausz, Opt. Lett. **31**, 1103 (2006).

8. C. Vozzi, G. Cirmi, C. Manzoni, E. Benedetti, F. Calegari, G. Sansone, S. Stagira, O. Svelto, S. De Silvestri, M. Nisoli, and G. Cerullo, Opt. Express **14**, 10109 (2006).

9. C. Vozzi, F. Calegari, E. Benedetti, S. Gasilov, G. Sansone, G. Cerullo, M. Nisoli, S. De Silvestri, and S. Stagira, Opt. Lett. **32**, 2957 (2007).

10. J. Tate, T. Auguste, H. G. Muller, P. Salières, P. Agostini, and L. F. DiMauro, Phys. Rev. Lett. **98**, 013901 (2007).

11. P. Colosimo, G. Doumy, C. I. Blaga, J. Wheeler, C. Hauri, F. Catoire, J. Tate, R. Chirla, A. M. March, G. G. Paulus, H. G. Muller, P. Agostini, and L. F. DiMauro, Nature Phys. **4**, 386 (2008) (and references therein).

12. V. S. Yakovlev, M. Ivanov, and F. Krausz, Opt. Express **15**, 15351 (2007).

13. E. J. Takahashi, T. Kanai, Y. Nabekawa, and K. Midorikawa, Appl. Phys. Lett. **93**, 041111 (2008).

14. E. J. Takahashi, T. Kanai, K. L. Ishikawa, Y. Nabekawa, and K. Midorikawa, Phys. Rev. Lett. **101**, 253901 (2008).

15. T. Popmintchev, M. C. Chen, O. Cohen, M. E. Grisham, J. J. Rocca, M. M. Murnane, and H. C. Kapteyn, Opt. Lett. **33**, 2128 (2008).

16. T. Popmintchev, M.-C. Chen, A. Bahabad, M. Gerrity, P. Sidorenko, O. Cohen, I. P. Christov, M. M. Murnane, and H. C. Kapteyn, Proc. Natl. Acad. Sci. USA **106**, 10516 (2009).

17. C. P. Hauri, R. B. Lopez-Martens, C. I. Blaga, K. D. Schultz, J. Cryan, R. Chirla, P. Colosimo, G. Doumy, A. M. March, C. Roedig, E. Sistrunk, J. Tate, J. Wheeler, L. F. DiMauro, and E. P. Power, Opt. Lett. **32**, 868 (2007).

18. L. Bergé, Opt. Express **16**, 21529 (2008).

19. J. Seres, E. Seres, A. J. Verhoef, G. Tempea, C. Streli, P. Wobrauschek, V. Yakovlev, A. Scrinzi, C. Spielmann, and F. Krausz, Nature **433**, 596 (2005).

20. O. D. Mücke, D. Sidorov, P. Dombi, A. Pugžlys, A. Baltuška, S. Ališauskas, V. Smilgevičius, J. Pocius, L. Giniūnas, R. Danielius, and N. Forget, Opt. Lett. **34**, 118 (2009).

21. O. D. Mücke, S. Ališsauskas, A. J. Verhoef, A. Pugžlys, A. Baltuška, V. Smilgevičius, J. Pocius, L. Giniūnas, R. Danielius, and N. Forget, Opt. Lett. **34**, 2498 (2009).

22. A. Varanavičius, A. Dubietis, A. Beržanskis, R. Danielius, and A. Piskarskas, Opt. Lett. **22**, 1603 (1997).

23. D. Kraemer, R. Hua, M. L. Cowan, K. Franjic, and R. J. D. Miller, Opt. Lett. **31**, 981 (2006).

24. D. Kraemer, M. L. Cowan, R. Hua, K. Franjic, and R. J. D. Miller, J. Opt. Soc. Am. B **24**, 813 (2007).

25. A. Baltuška, T. Fuji, and T. Kobayashi, Phys. Rev. Lett. **88**, 133901 (2002).

26. W. Koechner, *Solid-State Laser Engineering*, 6th edition (Springer, Berlin, 2006).

27. G. P. Agrawal, *Nonlinear Fiber Optics*, 4th edition (Academic Press, New York, 2007).

28. M. P. Kalashnikov, E. Risse, H. Searchönnagel, and W. Sandner, Opt. Lett. **30**, 923 (2005).

29. F. Verluise, V. Laude, J. P. Huignard, P. Tournois, and A. Migus, J. Opt. Soc. Am. B **17**, 138 (2000).